Biosensors and Bioelectronics 143 (2019) 111629

Contents lists available at ScienceDirect

Biosensors and Bioelectronics

journal homepage: www.elsevier.com/locate/bios

Bioinspired photonic barcodes for multiplexed target cycling and hybridization chain reaction

Dagan Zhang[a,b], Feika Bian[b], Lijun Cai[b], Tianfu Wang[a,**], Tiantian Kong[a,***], Yuanjin Zhao[a,b,*]

[a] Guangdong Key Laboratory of Biomedical Measurements and Ultrasound Imaging, Department of Biomedical Engineering, Shenzhen University, Shenzhen, 518060, China
[b] State Key Laboratory of Bioelectronics, School of Biological Science and Medical Engineering, Southeast University, Nanjing, 210096, China

ARTICLE INFO

Keywords:
Polydopamine
Barcode
Colloidal crystal
Target cycle amplification
miRNA

ABSTRACT

Multiplexed detection of microRNA (miRNA) is of great value in clinical diagnosis. Here, a new type of polydopamine (PDA) encapsulated photonic crystal (PhC) barcodes are employed for target-triggering cycle amplification and hybridization chain reaction (HCR) to achieve multiplex miRNA quantification. The PDA-decorated PhC barcodes not only exhibit distinctive structural color for different encoding miRNAs, they also can immobilize biomolecules, allowing subsequent reaction with amino-modified hairpin probes (H1). When the PDA-decorated PhC barcodes are used in assays, target miRNAs can be circularly used to initiate HCR for cycle amplification. Therefore, by tuning the structural colors of the PDA-integrated PhC, the multiplexed miRNA quantification could be realized. We demonstrate that our strategy for multiplexed detection of miRNA is reasonably accurate, reliable and repeatable, with a detection limit as low as 8.0 fM. Our results show that PDA encapsulated PhC barcodes as a novel platform offer a pathway toward the multiplex analysis of low-abundance biomarkers for biomedical assays.

1. Introduction

MicroRNAs (miRNAs) are small, noncoding RNA molecules with 18–25 nucleotides that are participated in the posttranscriptional regulation of gene expression and cell activities, including cell proliferation, and apoptosis (Calin and Croce, 2006; Esquela-Kerscher and Slack, 2006; Griffiths-Jones et al., 2008). The aberrant expression levels of miRNA are associated with tumor progression and metastasis, which can be used as valuable biomarkers for early diagnosis of diseases (Dong et al., 2013; Jing et al., 2015; Kooshapur et al., 2018). Therefore, the accurate and rapid detection of the amounts of miRNAs non-invasively is meaningful for early diagnosis of cancers and monitoring the efficacy during cancer therapy. However, the quantitative detection of miRNAs has remained a challenge, since they have low expression level in blood, difficult to extract/concentrate from blood samples and highly susceptible to degradation (Lu et al., 2016). To improve the sensitivity of microRNA detection, several amplification strategies have been developed for the quantification of miRNAs such as polymerase chain reaction (PCR) (Morrison et al., 2006), hybridization chain reaction (HCR) (Yang et al., 2012) and so on (Zhang et al., 2019; Yin et al., 2019). Although PCR can realize the detection of low-abundance miRNAs, its multiple thermal cycling and reliance on enzymes render it unsuited for high-throughput analysis (Zhang et al., 2016). In contrast, HCR is an isothermal, enzyme-free, one-step amplification process that mainly needs chain initiators and two hairpin nucleic acid probes; it is regarded as an important tool for nucleic acid amplification (Zhang et al., 2012). However, the common HCR does not involve the amplification of target cycle and thus fail to detect lower concentrations of miRNA in complicate clinical sample. In addition, most of these amplification methods for quantification of miRNAs are only carried out with single target test, which is usually not sufficient to guide diagnosis of lower concentrations of miRNA. Therefore, the development of a composite platform that can simultaneously detect multiplex miRNAs with high sensitivity and specificity is urgently needed.

To address the need, we propose an innovative HCR-integrated encoding carrier for multiplex, high-selectivity and high-sensitivity miRNAs screening. Encoding carrier such as planar microarrays (Murthy et al., 2008; Meng et al., 2015), suspension barcodes (Xu et al., 2018; Zhang and Khademhosseini, 2017), fluorescent molecules (Yang et al., 2019), quantum dots (Wang et al., 2002), graphical or shape-encoded microplates (Zheng et al., 2019) and photonic crystal (PhC) barcodes have been employed in multiplex detection of biomakers

* Corresponding author. Truncated: Sipailou 2, Xuanwu District, Nanjing, Jiangsu Province, China.
** Corresponding author.
*** Corresponding author.
E-mail addresses: tfwang@szu.edu.cn (T. Wang), ttkong@szu.edu.cn (T. Kong), yjzhao@seu.edu.cn (Y. Zhao).

https://doi.org/10.1016/j.bios.2019.111629
Received 15 July 2019; Received in revised form 21 August 2019; Accepted 22 August 2019
Available online 22 August 2019
0956-5663/

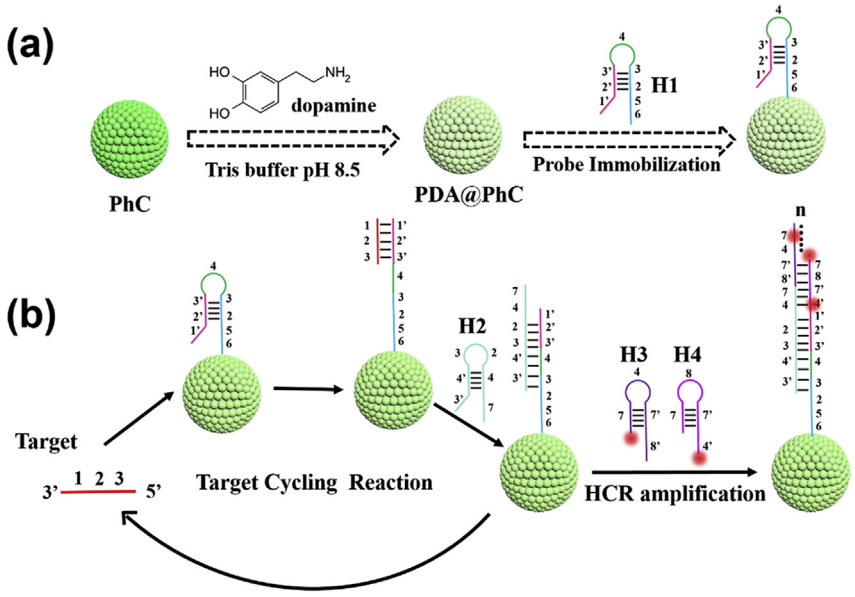

Fig. 1. (a) Schematic illustration of the preparation process of PDA-decorated PhC barcodes and probe immobilization. (b) Schematic illustration of the PDA-decorated PhC barcodes for miRNA detection based on target-triggering cycle amplification and HCR.

(Chen et al., 2017; Fu et al., 2017; Ge and Yin, 2011; Hou et al., 2014). Compared with other barcodes, PhC particles have distinct advantages, such as brilliant optical performance, remarkable encoding stability, free of any fluorescent background and photobleaching, which make them as a promising platform for multiplex detection of biomarkers (Bian et al., 2018, 2019; Cai et al., 2019; Xu et al., 2017, 2018; Wang et al., 2019; Hu et al., 2008). However, the effective means to surface-modify the PhC particles for biomolecules immobilization have been lacking, which limits the implementation of PhC particles for multiplex detection of biomolecules in practical samples (Xu et al., 2018; Liu et al., 2018).

In this paper, we integrated the target-triggering cycle amplification and HCR into the PDA decorated PhC particles for multiplex miRNAs quantification. Dopamine (DA), the composition of adhesive proteins in mussels (Cui et al., 2014; Lee et al., 2009; Li et al., 2017; Toma and Tawa, 2016), has attracted great attention as bio-adhesives (Ryu et al., 2018; Jung et al., 2018). It contains many catechols and quinones that enable us to modify the surface of PhC particles to immobilize biomolecules (Lee et al., 2009; Loget et al., 2013; Wood et al., 2013). Hence, as schemed in Fig. 1, we employed self-polymerization of DA to form PDA encapsulated PhC particles with abundant functional surface groups. Thus, the amino-modified hairpin-structured DNA probes (H1) could be easily immobilized on the surface of PDA-decorated PhC barcodes by Michael addition under mild condition. Once the target appeared, the target miRNAs could be circularly used to trigger HCR in the presence of H2, H3, H4; the final products of HCR that could be detected by measuring the fluorescent signal of PhC particles which is positively correlated with miRNAs concentration. More importantly, by utilizing different PDA-decorated PhC barcodes, multiplexed miRNA quantification could be realized. Our results indicated that the target-triggering cycle amplification and HCR combined with PDA-decorated PhC barcodes provided an unprecedented quantification platform for the multiplex detection of miRNAs with improved sensitivity and throughput. The presented strategy has important potentials for clinical applications, such as the early diagnosis of cancer.

2. Experimental methods

2.1. Preparation of PDA-decorated PhC barcodes

To prepare PDA-decorated silica colloidal crystal barcodes. First, the PhC barcodes were immersed into piranha solution overnight, and then washed with water. Next, 5.0 mL aliquot of as prepared 10 mM Tris-HCl solution (pH 8.5) containing 2.0 mg/mL DA solution was mixed with silica colloidal crystal barcodes under vigorous stirring for 6.0 h at room temperature. After the reaction, the brown colored PhC barcodes were obtained and carefully washed with deionized (DI) water several times and then ethanol to remove redundant PDA.

2.2. Probe immobilization

The sequences were heated to 95 °C for 2.0 min and then allowed to cool slowly to room temperature for 2.0 h before use in this work. The PDA-decorated barcodes were incubated with excessive amino-modified probes (H1) in 10 mM Tris-HCl buffer (pH 8.5) for 4.0 h to perform the probe immobilization at 37 °C in the constant shaker, the unreacted probes were rinsed with 10 mM Tris-HCl buffer. Then the different barcodes with corresponding probes were prepared successfully after washed with buffer solution.

2.3. Multiplex miRNAs quantification

Three kinds of PDA-decorated barcodes were incubated with excessive probes (0.10 μM) in 10 mM Tris-HCl buffer (pH 8.5) for 4.0 h at 37 °C in the constant shaker, respectively. Then three kinds of the probes for corresponding targets (miRNA-21, miRNA-210, and miRNA-155) were incubated with the three different PDA-decorated PhC barcodes (blue, green and red). Next, three kinds of 1.0 μL of targets miRNA (10×10^{-9} M), 1.0 μL of H2 (100×10^{-9} M) and 1.0 μL of CY3 decorated DNA hairpin (H3, H4) (150×10^{-9} M) were added to three barcodes in solution for 1.0 h at 37 °C in the constant shaker. Finally, the PDA-decorated PhC barcodes could be detected by fluorescence after washed three times with DI water.

3. Results and discussion

3.1. Design of the PDA-decorated PhC barcodes

In a typical experiment, the PhC barcodes were derived from the self-assemble of silica nanoparticles in microfluidic droplets. Subsequently PhC particles were dispersed into a DA solution in 10 mM Tris-buffer (pH 8.5) for 6.0 h with slight shake and then the PDA-

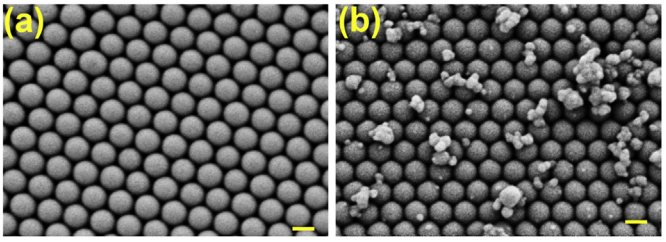

Fig. 2. SEM images: (a) the surface of a PhC particle; (b) the surface of a PDA-encapsulated PhC particle. Scale bar is 200 nm.

encapsulated PhC particles were obtained due to the self-polymerization of DA to form PDA layers which deposited on the surface of PhC particles (Fig. 1a). The PhC particles contained abundant functional groups after PDA decoration, and subsequent were further reacted with amino groups at a slightly basic pH via Schiff base formation or Michael addition without any complex chemical treatment for biomolecule immobilization. Therefore, the PDA-decorated PhC barcodes provided a versatile platform for a variety of functional molecules immobilization.

3.2. Fabrication of the PDA-decorated PhC barcodes

In order to fully illustrate the microstructure of the silica nanoparticles templates and the PDA-encapsulated PhC barcodes, scanning electron microscopy (SEM) was then utilized to characterize. As shown in Fig. 2a, it could be seen that monodispersed silica nanoparticles were self-assembled into a highly ordered hexagonal close-packed array from the high-resolution images of the surface of PhC. The process of DA self-polymerizes in basic solutions and the resulting PDA could deposit onto the PhC templates which could be confirmed in Fig. 2b. Moreover, the size of silica nanoparticles of PDA-PhC kept unchanged and still maintain a highly ordered structure. It was the highly ordered structure that endowed these encoding carriers with brilliant structural colors. Meanwhile, different structural colors could be obtained by adjusting the size of silica nanoparticles, thus realizing the characteristics of multiple encoding (Fig. 3a–c). This indicated that the PhC could serve as excellent barcodes for multiplexed analysis.

Note that, the high order periodic nanostructure of PhC particles was not affected by dopamine modification (Fig. 2b), because the characteristic reflection peak position of PhC particles mainly depends on the distance between the center of two neighboring silica nanoparticles and $n_{average}$ according to the formula Bragg's equation: $\lambda = 1.633\ d_{naverage}$. where λ refer to the reflection peak position, d is the center-to-center distance of adjacent silica nanoparticles, and $n_{average}$ is the average refractive index of the PhC particles. When the constitutes of PhC are kept unchanged, $n_{average}$ is constant, and thus the reflection peak value λ depends only on the size of the silica nanoparticles. Therefore, a series of different reflection spectra could be obtained by changing different diameter of silica nanoparticles.

Compared with the bare PhC barcodes assembled from the same size of silica nanoparticles, the structural color of the PDA-decorated PhC barcodes was more pronounced (Fig. 3d–f). Besides, the intensity of the reflection peak was dropped and the position the reflection peak was also slightly red-shifted (about 10 nm) after being wrapped by the PDA compared with that of the corresponding bare PhC as shown in Fig. 3g–i. Because the PDA deposited on the surface and even entered the interior of the PhC barcodes during the encapsulation process, part of the light scattering of PhC was absorbed by PDA as its broadband absorption which endowed it with the higher contrast and more prominent center spot after PDA modification. In a word, the PDA coating had little effect on the structural colors of the PhC barcodes to ensure

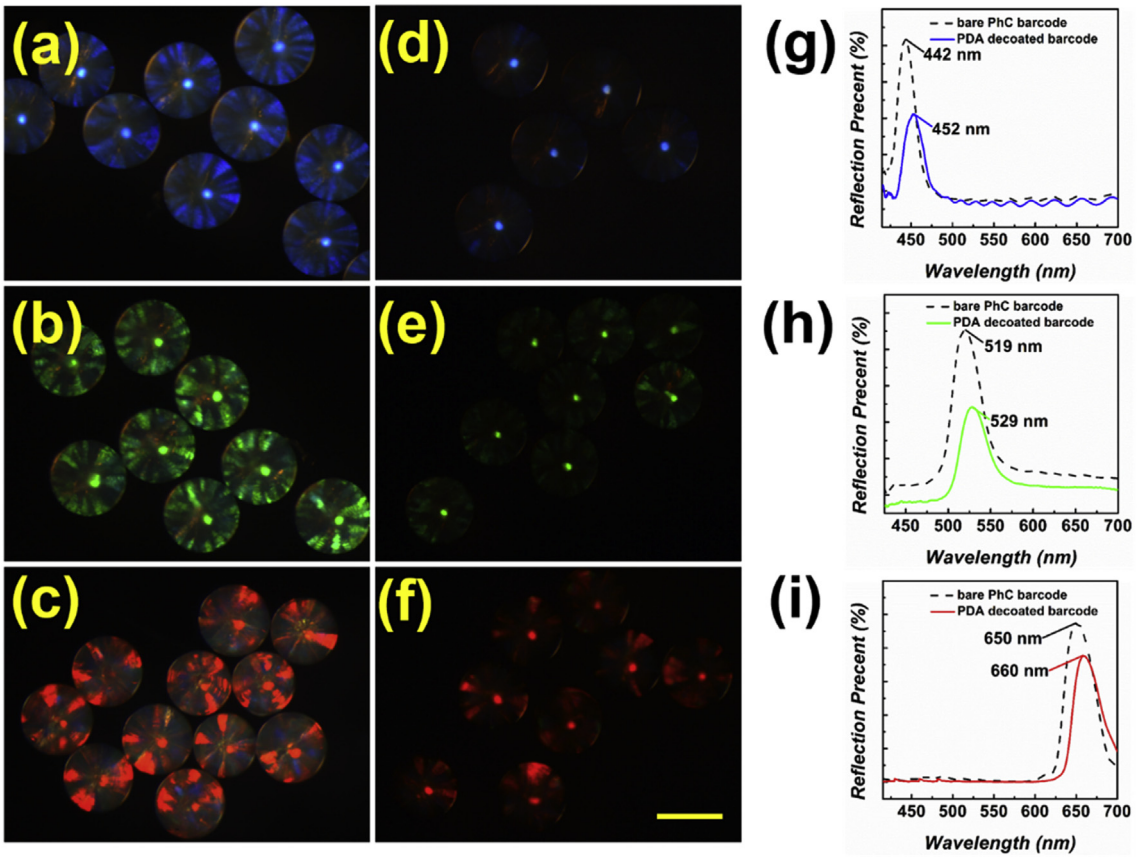

Fig. 3. (a–c) Reflection images of three kinds of PhC barcodes. (d–f) Reflection images of three kinds of PDA-decorated PhC barcodes. (g–i) Reflectionspectra of these three kinds of PhC barcodes before and after decorating with PDA. Scale bar is 200 μm.

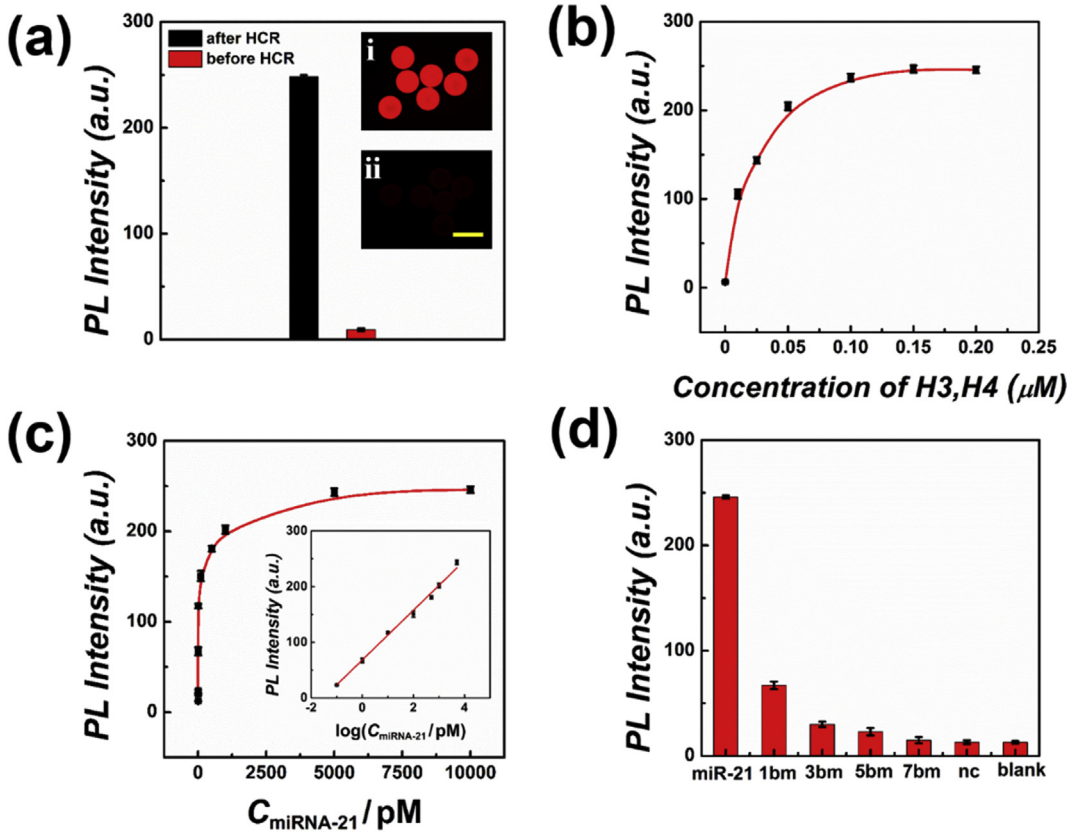

Fig. 4. (a) The Fluorescence intensity comparison before and after HCR amplification. (b) The relationship of the fluorescence intensity with the CY3-decorated H3, H4 concentration, 0.15×10^{-6} M is saturated concentration. (c)The relationship of the fluorescence intensity with miRNA-21 concentration. (d) The fluorescence statistics of PDA-decorated PhC barcodes-HCR products as a function of mutation level of miRNA-21. The error bars represent standard deviation for three replicated measurements.

that the PDA-PhC particles could still be used as an ideal barcodes carrier for multiplexed biodetection.

3.3. Feasibility detection and optimization of PDA-PhC particles

To evaluate the feasibility and application potential of the PDA-PhC particles as a platform for biodetection, the miRNA-21 was chosen as the targeting molecule. In our assay protocol (Fig. 1b), amino-modified hairpin nucleic acid probes were incubated with PDA-PhC barcodes under basic solution. And then the PDA-PhC barcodes functionalized with the hairpin probe DNA (H1) was exposed to a mixture of target miRNAs and three helper DNAs (H2, H3, H4), the hairpin-structured DNA probes (H1) were opened in the presence of target miRNAs to form a complex H1·target, after the complex H1·target hybridization with hairpin H2 by the strand displacement reaction, the complex H1·H2 was obtained and target was released to involve next cycle, meanwhile the resulting complex H1–H2 would trigger hybridization chain amplification reaction with CY3 labelled H3 and H4 to realize high sensitivity detection, the presence of miRNAs could be circularly used to trigger HCR, leading to long DNA copolymers for the amplification of DNA products to realize highly sensitivity detection. Therefore, the target recycling and self-assembly signal amplification strategy integrated into PDA decorated PhC barcodes which were used to strengthen the detected signal and its sensitivity. The signal amplification strategy was confirmed according to the fluorescence microscope images, the photoluminescence (PL) intensity at the barcode surface was measured. The results showed that the PL intensity increased by a factor of about 33 after HCR compared with before HCR when the concentration of the target reach to the maximum level (Fig. 4a), this result indicated that PDA-decorated PhC could be used to detect miRNA.

To improve the sensitivity of the miRNA detection on the PDA encapsulated PhC barcodes, the probe concentration was optimized. In these processes, the barcodes were incubated with different concentrations of probes H3 and H4 for miRNA-21 and then mixed with saturated synthetic target miRNA-21. It was found that the fluorescence intensity of PDA-decorated PhC barcodes gradually increased with the increasing of H3, H4 concentration and almost reached to maximum level when the hairpin probe concentration exceeded 150×10^{-9} M (Fig. 4b).

Incubation time as also an important parameters for the signal amplification performance, was optimized. As shown in Fig. S1, the PL intensity gradually increased and reached to maximum level with the extension of the incubation time from 0 to 60 min, followed with subsequently nearly kept constant after a short 10 min ligation. Therefore, a ligation time of 60 min was chosen as optimization incubation time to complete reaction in this study. Under these optimized conditions, different concentrations of miRNA-21 was investigated, the PL intensity of the PDA-decorated PhC particles was increased when the concentration of target miRNA-21 increased from 10^{-14} to 10^{-8} M and was linearly correlated to the logarithm of miRNA-21 concentration from 10^{-13} M to 5.0×10^{-9} M (Fig. 4c), and the relative standard deviations (RSD) were almost below 6.7%. The detection limit, calculated as three times the standard deviation of the blank divided by the slope, was 8.0 fM. Compared with the traditional fluorescence detection, the detection limit was lowered by more than three orders, thanks to target recycle amplification and HCR (Bian et al., 2018). In addition, In order to widen its application, two other kinds of miRNAs were investigated in 4 × SSC buffer with the PDA-decorated PhC particles, there were similar results (Figs. S2a and 2b). These results indicated that our method was both high sensitivity and could be useful for

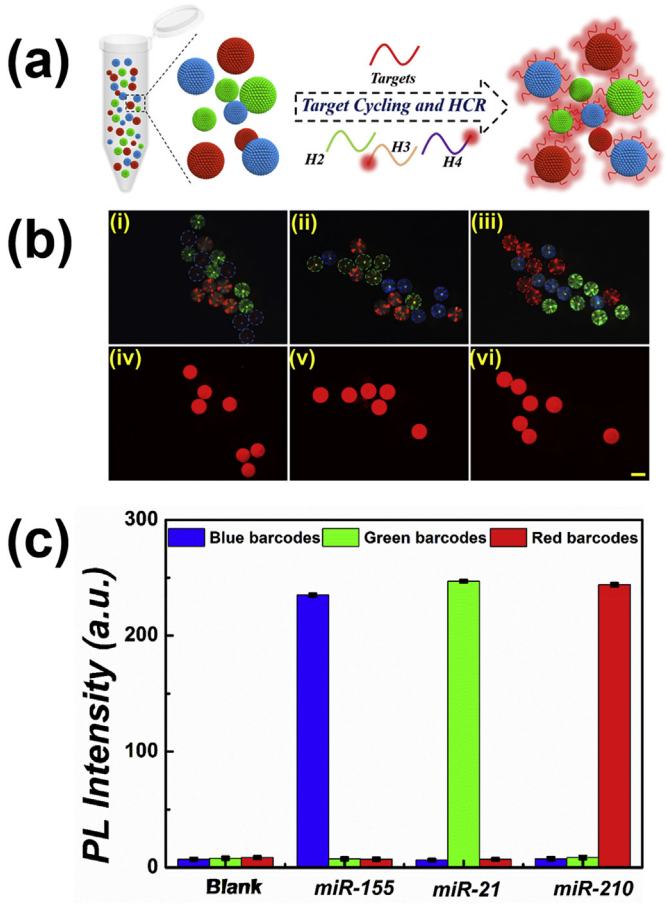

Fig. 5. (a) Schematic diagram of the specifcity of PDA-decorated PhC barcodes for multiplex miRNA detection; (b) optical microscopy images (i-iii) and fluorescence images (iv-vi) of three kinds of PDA-decorated PhC barcodes after incubating with three different of miRNA; Scale bar is 200 μm. (c) The fluorescence statistics after incubating targets with three different PDA-decorated PhC barcodes.

miRNA detection.

A great challenge of the miRNAs assay was to distinguish the concomitant miRNAs with high similarity. To further investigate the specificity of the detection method proposed, four different mutated sequences (Table S1) were performed in our detection method. As shown in Fig. 4d, the fluorescence signals from the PDA-decorated PhC particles effectively discriminated between the target sequence and the mutated sequences. The results showed that the PL intensities of the 1-base and 3-base mutations were only about 27% and 13% of that for perfect complementary target DNA at the same concentration, respectively. When the mutated sequences reach to seven base mutations, the PL intensity was reduced to that of a fully non-complementary sequence (nc). Besides, two other kinds of miRNA-155 and miRNA-210 were specifcity tested, which showed similar results (Figs. S3a and 3b). These results demonstrated that our strategy had both high sensitivity and high specificity. Therefore, the PDA-decorated PhC barcodes integrated with the target-triggering cycle amplification and HCR strategy not only offered an excellent platform for detecting low-abundance miRNA with high accuracy and but also the good performance to discriminate perfect complementary target and the mismatched targets which endowed it great potential for single nucleotide polymorphism analysis.

3.4. Multiplexed detection by PDA-integrated PhC barcodes

Finally, we demonstrated multiplexed detection of miRNA-21, miRNA-155, and miRNA-210 with PDA-integrated PhC barcodes, respectively. These miRNAs were found to exhibit high expression in pancreatic cancer so that multiplex detection of these miRNAs had great of value in clinical diagnosis. Hence, three kinds of barcodes with the characteristic reflection peaks at 450 nm (blue), 519 nm (green), and 650 nm (red) were utilized for the simultaneous quantification of the three kinds of miRNAs. The red, green, and blue PDA-decorated PhC barcodes were decorated with different corresponding probes, respectively, and then incubated with the mixed solution including one of three kinds of miRNA target, H2 and the CY3 decorated H3, H4 under the same conditions. Because of the specifcity binding between the targets and the corresponding probes, the fluorescence signal were only observed on the barcodes that could couple with the corresponding miRNA target after HCR amplification, as shown in Fig. 5. To further demonstrate the multiplexing capability and accuracy. The barcodes were also incubated with two or three kinds of target miRNA to detect and distinguish different targets in a single measurement (Figs. S4–S6). These results indicated that the PDA encapsulated PhC barcodes integrated with target-triggering cycle amplification and HCR were potential valuable performance with a high specificity, high sensitivity and anti-interference for multiplex miRNAs detection in clinical setting. These multiplex properties are in accordance with the previously literatures (Cai et al., 2019; Bian et al., 2019). Therefore, the presented strategy could as a novel potential platform for multiplexed biomarkers analysis and disease diagnosis.

4. Conclusion

In conclusion, we have developed a novel PDA-decorated PhC barcodes by target-triggering cycle amplification and HCR for multiplexed microRNA quantification. The PhC barcodes contained a number of groups to immobilize biomolecule, enabled by PDA decoration, with the preservation of coding characteristics. By implementing PDA-decorated PhC barcodes with target-triggering cycle amplification and HCR, it was demonstrated that three kinds of pancreatic cancer-associated miRNAs detection could be achieved simultaneously with high sensitivity and selectivity, in which the detection limit was 8.0 fM. We anticipate that the PDA-decorated PhC barcodes are a versatile sensing platform for a wide range of practical applications, such as early diagnosis of diseases. Furthermore, the encoding carrier is only suitable for multiplex detection by fluorescence imaging; more work should be extended to colorimetry in the future.

Author contributions

Y.J.Z. conceived the conceptualization and designed the experiment; D.G.Z. carried out the experiments; D.G.Z., F.K.B. and Y.J.Z. analyzed data and wrote the paper; L.J.C., and T.F.W, T.T.K contributed to scientific discussion of the article.

Notes

The authors declare no competing financial interest.

CRediT authorship contribution statement

Dagan Zhang: Data curation, Formal analysis, Writing - original draft. **Feika Bian:** Formal analysis, Writing - original draft. **Lijun Cai:** Formal analysis, Writing - original draft. **Tianfu Wang:** Methodology, Investigation, Resources, Writing - review & editing. **Tiantian Kong:** Methodology, Investigation, Resources, Writing - review & editing. **Yuanjin Zhao:** Conceptualization, Funding acquisition, Project administration, Resources, Supervision.

Declaration of competing interest

The authors declare that they have no known competing financial

interests or personal relationships that could have appeared to influence the work reported in this paper.

Acknowledgements

This work was supported by the National Key Research and Development Program of China (2017YFA0700404), the National Natural Science Foundation of China (grants 51522302 and 21473029), the NSAF Foundation of China (grant U1530260), the Natural Science Foundation of Jiangsu (Grant no. BE2018707), the Fundamental Research Funds for the Central Universities, and the Scientific Research Foundation of Southeast University.

Appendix A. Supplementary data

Supplementary data to this article can be found online at https://doi.org/10.1016/j.bios.2019.111629.

References

Bian, F., Sun, L., Cai, L., Wang, Y., Zhao, Y., Wang, S., Zhou, M., 2019. Biosens. Bioelectron. 133, 199–204.
Bian, F., Wu, J., Wang, H., Sun, L., Shao, C., Wang, Y., Li, Z., Wang, X., Zhao, Y., 2018. Small 14 (52), 1803551.
Cai, L., Bian, F., Sun, L., Wang, H., Zhao, Y., 2019. Lab Chip 19 (10), 1783–1789.
Calin, G.A., Croce, C.M., 2006. Nat. Rev. Cancer 6 (11), 857–866.
Chen, K., Fu, Q., Ye, S., Ge, J., 2017. Adv. Funct. Mater. 27 (43), 1702825.
Cui, W., Li, M., Liu, J., Wang, B., Zhang, C., Jiang, L., Cheng, Q., 2014. ACS Nano 8 (9), 9511–9517.
Dong, H., Lei, J., Ding, L., Wen, Y., Ju, H., Zhang, X., 2013. Chem. Rev. 113 (8), 6207–6233.
Esquela-Kerscher, A., Slack, F.J., 2006. Nat. Rev. Cancer 6 (4), 259–269.
Fu, F., Chen, Z., Zhao, Z., Wang, H., Shang, L., Gu, Z., Zhao, Y., 2017. Proc. Natl. Acad. Sci. U.S.A. 114 (23), 5900–5905.
Ge, J., Yin, Y., 2011. Angew. Chem. Int. Ed. 50 (7), 1492–1522.
Griffiths-Jones, S., Saini, H.K., van Dongen, S., Enright, A.J., 2008. Nucleic Acids Res. 36, D154–D158 Database issue).
Hou, J., Zhang, H., Yang, Q., Li, M., Song, Y., Jiang, L., 2014. Angew. Chem. Int. Ed. 53 (23), 5791–5795.
Hu, X., Huang, J., Zhang, W., Li, M., Tao, C., Li, G., 2008. Adv. Mater. 20 (21), 4074–4078.
Jing, Z., Han, W., Sui, X., Xie, J., Pan, H., 2015. Cancer Lett. 356 (2 Pt B), 332–338.
Jung, H.S., Cho, K.J., Seol, Y., Takagi, Y., Dittmore, A., Roche, P.A., Neuman, K.C., 2018. Adv. Funct. Mater. 28 (33), 1801252.
Kooshapur, H., Choudhury, N.R., Simon, B., Muhlbauer, M., Jussupow, A., Fernandez, N., Jones, A.N., Dallmann, A., Gabel, F., Camilloni, C., Michlewski, G., Caceres, J.F., Sattler, M., 2018. Nat. Commun. 9 (1), 2479.
Lee, H., Rho, J., Messersmith, P.B., 2009. Adv. Mater. 21 (4), 431–434.
Li, J., Baird, M.A., Davis, M.A., Tai, W., Zweifel, L.S., Adams Waldorf, K.M., Gale Jr., M., Rajagopal, L., Pierce, R.H., Gao, X., 2017. Nat. Biomed. Eng. 1 (6), 0082.
Liu, P., Chen, J., Zhang, Z., Xie, Z., Du, X., Gu, Z., 2018. Nanoscale 10 (8), 3673–3679.
Loget, G., Wood, J.B., Cho, K., Halpern, A.R., Corn, R.M., 2013. Anal. Chem. 85 (21), 9991–9995.
Lu, W., Chen, Y., Liu, Z., Tang, W., Feng, Q., Sun, J., Jiang, X., 2016. ACS Nano 10 (7), 6685–6692.
Meng, J., Zhang, P., Zhang, F., Liu, H., Fan, J., Liu, X., Yang, G., Jiang, L., Wang, S., 2015. ACS Nano 9 (9), 9284–9291.
Morrison, T., Hurley, J., Garcia, J., Yoder, K., Katz, A., Roberts, D., Cho, J., Kanigan, T., Ilyin, S.E., Horowitz, D., Dixon, J.M., Brenan, C.J., 2006. Nucleic Acids Res. 34 (18), e123.
Murthy, B.R., Ng, J.K., Selamat, E.S., Balasubramanian, N., Liu, W.T., 2008. Biosens. Bioelectron. 24 (4), 723–728.
Ryu, J.H., Messersmith, P.B., Lee, H., 2018. ACS Appl. Mater. Interfaces 10 (9), 7523–7540.
Toma, M., Tawa, K., 2016. ACS Appl. Mater. Interfaces 8 (34), 22032–22038.
Wang, D., Rogach, A.L., Caruso, F., 2002. Nano Lett. 2 (8), 857–861.
Wang, Y., Shang, L., Bian, F., Zhang, X., Wang, S., Zhou, M., Zhao, Y., 2019. Small 15 (13), e1900056.
Wood, J.B., Szyndler, M.W., Halpern, A.R., Cho, K., Corn, R.M., 2013. Langmuir 29 (34), 10868–10873.
Xu, W., Li, Z., Yin, Y., 2018. Small 14 (35), 1801083.
Xu, Y., Wang, H., Luan, C., Fu, F., Chen, B., Liu, H., Zhao, Y., 2018. Adv. Funct. Mater. 28 (1), 1704458.
Xu, Y., Zhang, X., Luan, C., Wang, H., Chen, B., Zhao, Y., 2017. Biosens. Bioelectron. 87, 264–270.
Yang, L., Liu, C., Ren, W., Li, Z., 2012. ACS Appl. Mater. Interfaces 4 (12), 6450–6453.
Yang, M., Liu, Y., Jiang, X., 2019. Chem. Soc. Rev. 48 (3), 850–884.
Yin, K., Zeng, X., Liu, W., Xue, Y., Li, X., Wang, W., Song, Y., Zhu, Z., Yang, C., 2019. Anal. Chem. 91 (9), 6003–6011.
Zhang, B., Liu, B., Tang, D., Niessner, R., Chen, G., Knopp, D., 2012. Anal. Chem. 84 (12), 5392–5399.
Zhang, D., Gao, B., Zhao, C., Liu, H., 2019. Langmuir 35 (1), 248–253.
Zhang, Y., Li, Q., Guo, L., Huang, Q., Shi, J., Yang, Y., Liu, D., Fan, C., 2016. Angew. Chem. Int. Ed. 55 (40), 12450–12454.
Zhang, Y.S., Khademhosseini, A., 2017. Science 356 (6337), eaaf3627.
Zheng, K., Chen, C., Chen, X., Xu, M., Chen, L., Hu, Y., Bai, Y., Liu, B., Yan, C., Wang, H., Li, J., 2019. Biosens. Bioelectron. 132, 47–54.